RSC Advances

PAPER

View Article Online
View Journal | View Issue

Cite this: *RSC Adv.*, 2015, **5**, 14637

Utilization of the microwave electric or magnetic field in the synthesis of monometallic and bimetallic nanoparticles

Takuya Sumi, Ralf Dillert† and Satoshi Horikoshi*

Received 9th January 2015
Accepted 21st January 2015

DOI: 10.1039/c5ra00452g

www.rsc.org/advances

The wet synthesis of mono-disperse Ag, Ag–Ni, and Pd–Ag nanoparticles has been performed employing glycol solutions containing $[Ag(NH_3)_2]^+$ and a second metal cation Mn^+ (M = Ag, Na, Al, Ni or Pd) under microwave irradiation in a predominately electric (*E*-) or a predominately magnetic (*H*-) field. No specific effects of the microwave *E*-field and *H*-field on the rate of product formation have been observed. But the synthesis of Ag–Ni alloy particles in the *E*-field and the *H*-field resulted in products with different particle size distribution, thus possibly indicating specific field effects.

Introduction

Microwave heating being an efficient heating method based on the interaction between the electromagnetic field of the microwave and chemical substances has attracted considerable attention in recent years. The application of microwave heating to accelerate the rate of chemical reactions is an increasing field of scientific research as documented by the rapidly increasing number of publications.

In the field of organic synthesis, microwave heating has been reported to be advantageous with respect to reaction time, chemical yield and purity of the products[1–3] being obtained by employing microwave rapid, uniform, and selective heating.[4]

The preparation of metal nanoparticles is another major field of microwave application.[5] The synthesis of many metal nanoparticles such as Au,[6–9] Ag,[10–13] Pt,[10] Ni,[11,14–16] Co,[11] and Fe[11] was performed by the microwave method. In comparison with conventional heating methods such as convective heating employing an oil-bath or an electric heater, the microwave heating of the precursor solutions allows not only shorter reaction time but also the formation of uniform particles with a narrow distribution of particle size.[13] Moreover, the microwave method facilitates the synthesis of bimetallic nanoparticles, nanoalloys, and nanocomposites such as core–shell particles.[17–23]

But the specific features of the microwave electromagnetic waves have not been examined in the metal nanoparticle synthesis. In particular, the impact of the microwave magnetic field on the heating of matter has almost been overlooked. In an early report we have shown that microwave irradiation of aqueous electrolyte solutions at a position within the microwave cavity having a predominant electric field (*E*-field) or a predominant magnetic field (*H*-field) resulted in differences in the heating rate of the solutions. The increase of the temperature during microwave irradiation of aqueous solutions with higher electrolyte concentration can be faster by *H*-field than by *E*-field irradiation. This effect has been explained with a Joule loss resulting from an eddy current induced by the microwave's alternating magnetic field.[24]

In this paper, the interference of the polyol synthesis of silver-containing nanoparticles by the microwave *E*-field and *H*-field was investigated. To investigate the field effects the synthesis has been performed in solutions containing Ag ions and additionally diamagnetic or paramagnetic (Ni^{2+}) ions.

Experimental section

Setup of microwave apparatus

The microwave irradiation setup with the single-mode cavity TE_{103} (transverse electric 103 mode), used to irradiate the reactor contents included a short plunger, an iris, a three-stub tuner, a power monitor and an isolator (schematically illustrated in Fig. 1). The continuous microwave radiation was generated from a 2.45 GHz microwave semiconductor generator (Fuji Electronic Industrial Co. Ltd.; GNU-201AA; maximal input power, 200 W). The resonance of the microwaves was adjusted with the iris and the short plunger at 1.5 cycles. Heating of the sample solution (1 mL) was achieved by positioning a cylindrical quartz reactor (external diameter = 5.0 mm; internal diameter = 4.0 mm) in the single-mode microwave apparatus as depicted in Fig. 1 either at the position of maximal *E*-field density or at the maximal *H*-field within the waveguide. The wavelength of propagation of the microwaves in the TE_{103} mode

Department of Material & Life Science, Faculty of Science and Technology, Sophia University, 7-1 Kioicho, Chiyodaku, Tokyo 102-8554, Japan. E-mail: horikosi@sophia.ac.jp

† During a leave of absence from the Institute of Technical Chemistry of the Gottfried Wilhelm Leibniz University, Hannover, Germany.

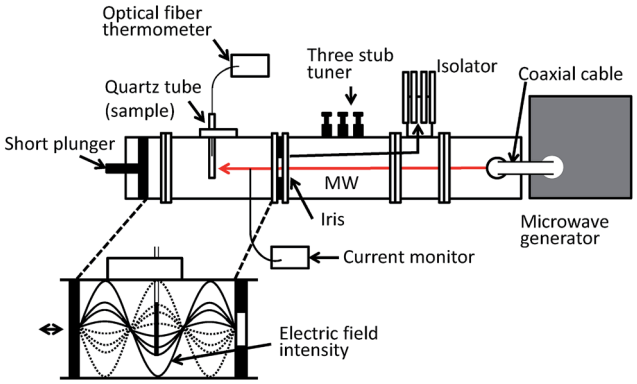

Fig. 1 Details of the experimental setup and the position of the samples in the single-mode microwave resonator. In this illustration, the sample is fit on the *E*-field position where the microwave electric field intensity has its maximum.

within the waveguide was *ca.* 14.78 cm, estimated from eqn (1):[25]

$$\lambda = \frac{\lambda_o}{\sqrt{1 - (\lambda_o/2b)^2}} \quad (1)$$

where λ is the wavelength in the waveguide, and $b = 10.92$ cm is the height of the waveguide. The wavelength in vacuum, $\lambda_{o(2.45\ GHz)} = c/f$, was calculated using the speed of light, $c = 2.9979 \times 10^{10}$ cm s^{-1}, and the microwave frequency, $f = 2.45$ GHz $= 2.45 \times 10^9$ s^{-1}, to be 12.24 cm. The maximal position of the *E*-field from the iris was located at 3/4 the wavelength of the standing wave in the waveguide, namely 11.09 cm. The maximal position of the *H*-field from the iris was at 1/2 the wavelength of the standing wave in the waveguide, namely 7.39 cm.[26] The inset in Fig. 1 illustrates the distribution of the *E*-field and *H*-field components of the microwave radiation inside the waveguide in single-mode operation under resonant conditions.[27]

The distribution of the *E*- and *H*-field inside the waveguide was calculated by using the COMSOL Multiphysics 4.3a program with RF module. The results of the calculation (Fig. 2) were confirmed by measuring the *E*-field density using a current monitor.

Synthesis of nanoparticles

Silver nitrate ($AgNO_3$), sodium nitrate ($NaNO_3$), aluminium nitrate ($Al(NO_3)_3 \cdot 9H_2O$), nickel nitrate ($Ni(NO_3)_2 \cdot 6H_2O$), palladium nitrate ($Pd(NO_3)_2$), NH_3 (28% aqueous solution), polyvinylpyrrolidone (PVP), and ethylene glycol (EG) were purchased from Wako Pure Chemicals Industry, Ltd., and used as received. Ultrapure water (≧18.2 MΩ cm) was used as solvent for the metal compounds.

Mono- and bi-metallic nanoparticles were prepared using the following procedure: 3.14 g (18 mM) of $AgNO_3$ was dissolved in 20 mL pure water and stirred for 1 h. Then, 6 mL of the NH_3 solution (310 mM) was added and stirred to prepare an aqueous $[Ag(NH_3)_2]^+$ complex solution. 50 μL of an aqueous $M(NO_3)_x$ (M = Ag, Al, Na, Ni, or Pd) solution (0.5 M) was dissolved in 5 mL of ethylene glycol. Subsequently, 50 μL of the $[Ag(NH_3)_2]^+$ complex solution and PVP (0.3 g) as the stabilizing reagent were added to the ethylene glycol solutions. Aliquots (1 mL) of these $[Ag(NH_3)_2]^+/M(NO_3)_x$ solutions were microwave irradiated at *E*-field or *H*-field position. The temperature of the solutions was measured by using an optical fiber thermometer (Anritsu Meter Co., Ltd.), which does not absorb microwave radiation. The microwave irradiation was turned off when the irradiated solutions became colored.

UV-visible absorption spectra of the irradiated solutions were recorded employing a JASCO UV-visible spectrophotometer V-660. Mean particle diameters, particle size distribution, and morphology were determined by using a bright-field transmission electron microscope (HITACHI High-Technology Co. H-7650 electron microscope).

Results and discussion

Pure Ag as well as bimetallic Ag/Ni and Ag/Pd nanoparticles have been synthesized from precursor solutions containing ethylene glycol as the reductant by heating both at the position of predominant (maximal) *E* field and of predominant (maximal) *H* field. Differences in the heating rate and the maximum temperature achieved after prolonged microwave irradiation became obvious. As a typical example, the temperature profiles of solutions containing $[Ag(NH_3)_2]^+$ and Ni^{2+} ion are shown in Fig. 3. The solid line in Fig. 3 describes the temperature change under *E*-field (80 W) irradiation while the dashed line is the result obtained under *H*-field (140 W) irradiation. The heating rate using the magnetic field was found to be lower than using *E*-field irradiation and the temperature did not exceed 85 °C. By contrast, *E*-field heating can heat the solution easily to 135 °C.

The thermal energy P produced per unit volume from the conversion of microwave radiation can be calculated from eqn (2),[28]

$$P = \frac{1}{2}\sigma|E|^2 + \pi f \varepsilon_0 \varepsilon_r''|E|^2 + \pi f \mu_0 \mu_r''|H|^2 \quad (2)$$

where $|E|$ and $|H|$ denote the strength of the microwaves' electric and magnetic fields, respectively; σ is the electrical conductivity; f is the frequency of the microwaves; ε_0 is the permittivity in vacuum; ε'' is the dielectric loss factor; μ_0 is the magnetic permeability in vacuum; and μ'' is the magnetic loss. In accordance with this equation, the microwave *E*-field results in dielectric and Joule heating (given by the two first summands of eqn (2)) of the reaction mixture. On the other hand, only Joule heating advances in the *H*-field (third summand in eqn (2)). Therefore, a difference in the heating rate and temperature of a sample under *E*-field and *H*-field irradiation is expected.

As it becomes obvious from Table 1 in all experimental runs heating of the solutions by the microwave *H*-field resulted in significantly lower temperatures than heating in the *E*-field even though a higher microwave power was employed to generate the *H*-field. It is assumed that the main heating mechanism of the reaction solution employing *E*-field irradiation is dielectric

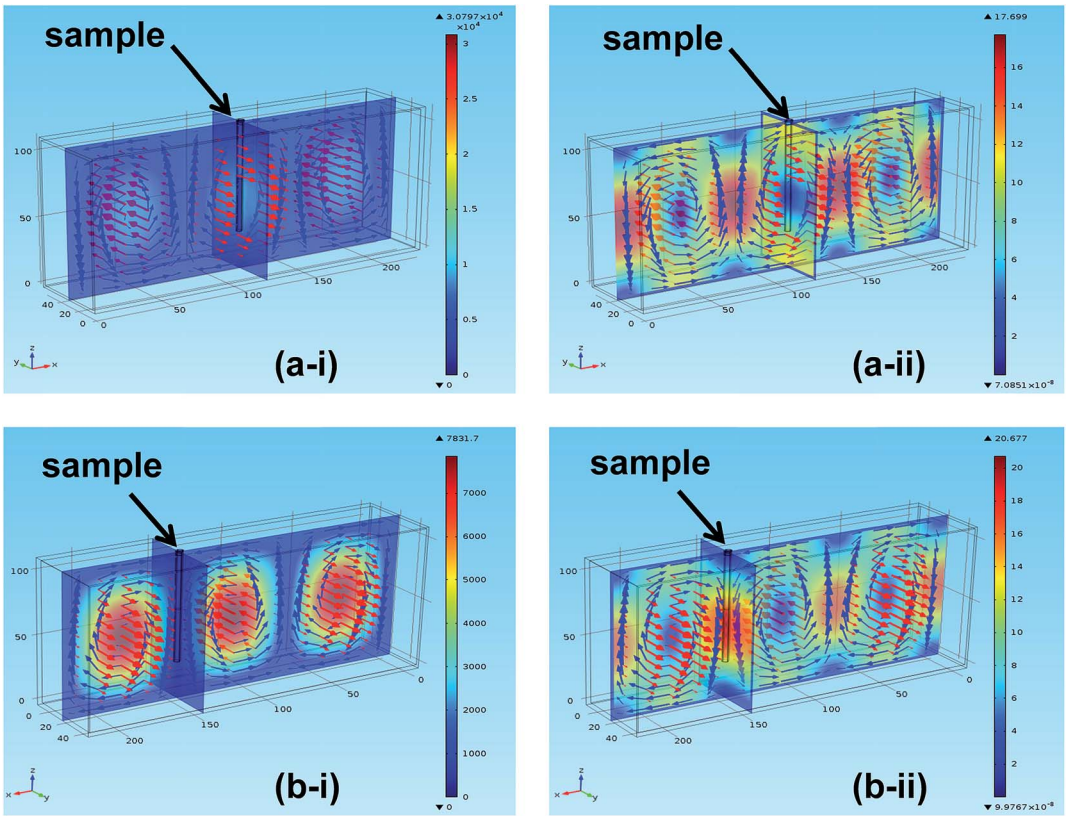

Fig. 2 Illustrations of the electromagnetic field in the waveguide calculated employing COMSOL Multiphysics software, and depicting the distribution of (a-(i)) the *E*-field and (a-(ii)) the *H*-field at *E*-field condition, and (b-(i)) the *E*-field and (b-(ii)) the *H*-field at *H*-field condition.

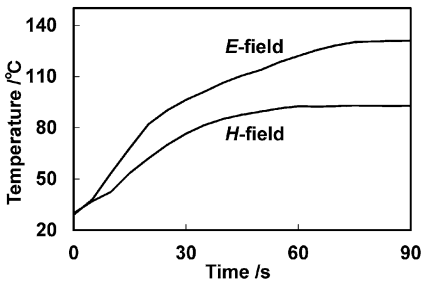

Fig. 3 Temperature profiles of solutions containing $[Ag(NH_3)_2]^+$ and Ni^{2+} ion under *E*-field (solid line) and *H*-field (dashed line) irradiation condition.

Table 1 The maximum temperature of the different solutions under investigation observed under microwave *E*- or *H*-field irradiation

	Maximum temperature/°C	
Precursor solution	*E*-field (80 W)	*H*-field (140 W)
$[Ag(NH_3)_2]NO_3$	135	82
$[Ag(NH_3)_2]NO_3/AgNO_3$	135	82
$[Ag(NH_3)_2]NO_3/Al(NO_3)_3$	135	84
$[Ag(NH_3)_2]NO_3/NaNO_3$	135	85
$[Ag(NH_3)_2]NO_3/Pd(NO_3)_2$	135	85
$[Ag(NH_3)_2]NO_3/Ni(NO_3)_2$	135	85

heating being more efficient than Joule heating occurring under *H*-field irradiation.[24]

The UV-visible absorption spectra of solutions and suspensions obtained by heating of solutions initially containing the $[Ag(NH_3)_2]^+$ complex solution as the only precursor of Ag nanoparticles, and solutions containing a mixture of $[Ag(NH_3)_2]^+$ with Ag^+, Al^{3+} or Na^+ in the microwave *E*-field to temperatures exceeding 90 °C are presented in Fig. 4. UV-visible absorption spectra of solutions and suspensions sampled after microwave irradiation of the pristine $[Ag(NH_3)_2]^+$ complex solution are shown in Fig. 4(a). A strong absorption peak centered at 420 nm becomes obvious for a solution heated to 120 °C. This peak at around 420 nm is attributed to the surface plasmon resonance (SPR) band being a typical feature of solutions containing silver nanoparticles.[29–32] In an experimental run at 110 °C no SPR was observed clearly indicating that no Ag nanoparticles have been formed. Fig. 4(b) depicts the optical absorption of an irradiated solution containing both $[Ag(NH_3)_2]^+$ and $AgNO_3$ heated to 90 °C and 105 °C under microwave *E*-field. In these experimental runs the SPR observed at 420 nm indicates nanoparticles formation at a temperature of 105 °C being significantly lower than the temperature required for Ag nanoparticle formation from the pristine $[Ag(NH_3)_2]^+$ complex solution. On the other hand, experimental results obtained with $[Ag(NH_3)_2]^+$ complex solutions containing Al and Na ions showed no influence of the additional solute on the

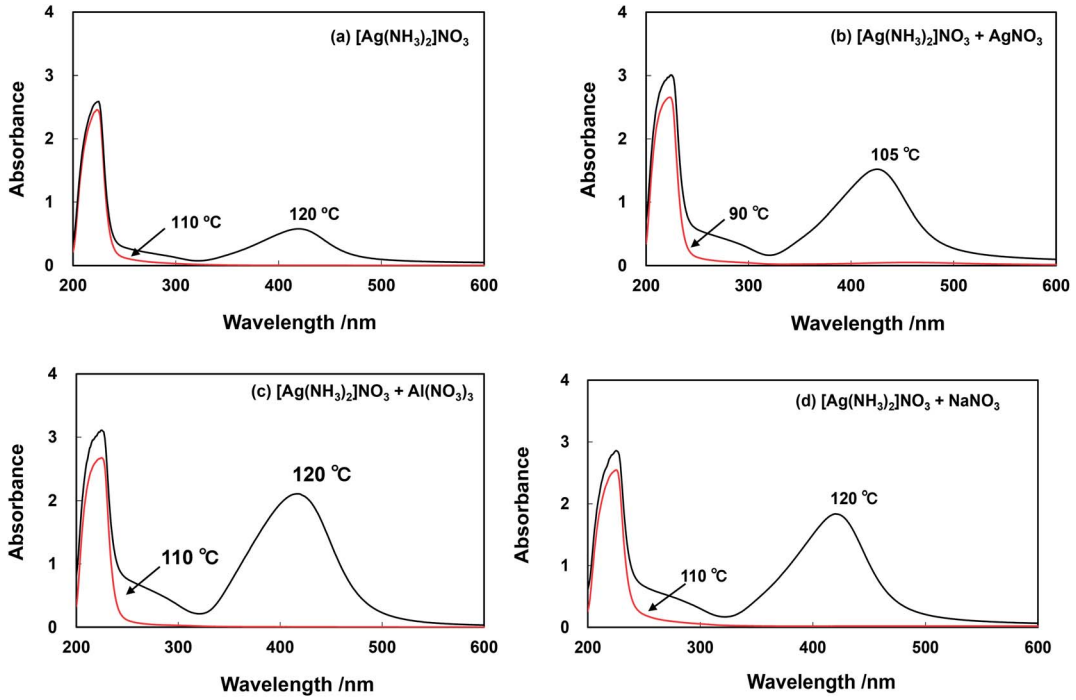

Fig. 4 UV-visible absorption spectra of solutions (eight fold dilution) containing Ag^{+} and M^{n+} ion heated in the microwave *E*-field. (a) $[Ag(NH_3)_2]NO_3$ (b) $[Ag(NH_3)_2]NO_3/AgNO_3$, (c) $[Ag(NH_3)_2]NO_3/Al(NO_3)_3$ (d) $[Ag(NH_3)_2]NO_3/NaNO_3$.

temperature required for Ag nanoparticle formation, *i.e.*, Ag nanoparticle formation only occurs at temperatures higher than 110 °C. The presence of Al^{3+} ion in $[Ag(NH_3)_2]^{+}$ solutions, which were microwave heated to a temperature ranging between 120 and 130 °C, resulted in spectra having a SPR peak centered at 420 nm (Fig. 4(c)). The reaction of the precursor solution containing added $NaNO_3$ at temperatures between 110 and 120 °C resulted in product suspensions showing a SPR peak centered at 421 nm (Fig. 4(d)). It has to be noted again that under *H*-field irradiation the temperature of the solutions mentioned above did not rise to values >85 °C during the experimental runs performed here. Consequently, no nanoparticle formation was observed under *H*-field irradiation.

The UV-visible absorption spectra of solutions and suspensions obtained by microwave heating of solutions initially containing a mixture of $[Ag(NH_3)_2]^{+}$ and Pd or Ni ions are presented in Fig. 5. The microwave irradiation of both glycol solutions containing Pd as well as Ni ions at *E*-field position resulted in the appearance of a SPR peak at a bulk temperature of 80 °C (Fig. 5). The SPR peaks of the Pd-containing and the Ni-containing suspension are centered at 440 and 432 nm, respectively, indicating the formation of Ag-containing nanoparticles at this significantly lower temperature. Since a bulk temperature of 80 °C is accessible by *H*-field irradiation (*cf.* Table 1) the formation of these nanoparticles as evinced by the SPR peaks (Fig. 5) was consequentially observed under heating at *H*-field position.

Microwave irradiation of a glycol solution containing $[Ag(NH_3)_2]^{+}/Pd(NO_3)_2$ resulted in the formation of a Ag–Pd bimetallic suspension showing a significantly higher absorption

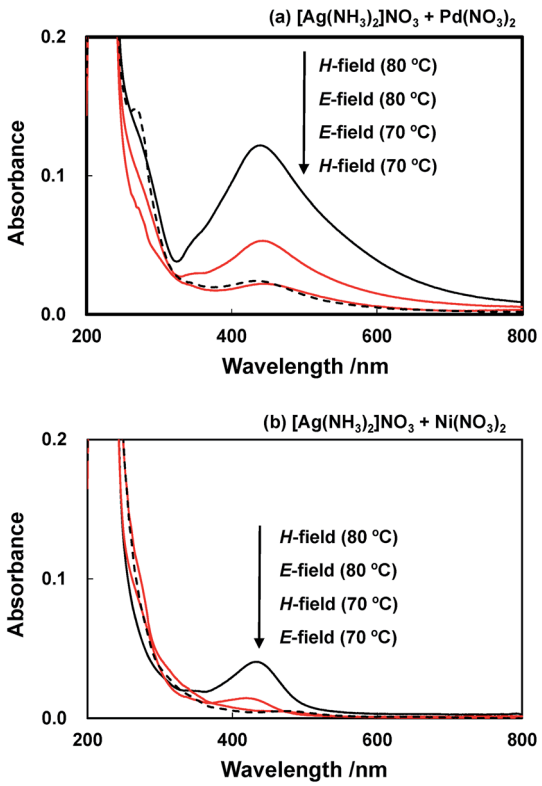

Fig. 5 UV-visible absorption (twenty fold dilution) spectra of solutions containing Ag^{+} and M^{n+} ion heated in the microwave *E*- and *H*-field. (a) $[Ag(NH_3)_2]NO_3/Pd(NO_3)_2$ (b) $[Ag(NH_3)_2]NO_3/Ni(NO_3)_2$.

peak at 440 nm (Fig. 5(a)) when compared with that of the Ag–Ni sample (Fig. 5(b)) indicating that Pd is promoting the reduction reaction. The spectra of the microwave irradiated bimetallic $[Ag(NH_3)_2]^+/Ni(NO_3)_2$ solutions show a surface plasmon band centered at 432 nm (Fig. 5(a)) having a peak height ten times lower than that of the Ag–Al sample, and being red shifted in comparison to the solution containing monometallic Ag nanoparticles. It is known that the UV-vis spectra of pure Ni nanoparticles show no peaks at wavelengths >250 nm,[33,34] therefore, the signal observed here has to be attributed to the presence of Ag–Ni nanoparticles. In comparison with Ag nanoparticles for both alloys a shift of the absorption band to longer wavelength of decreased intensity is observed in accordance with reported data.[34–37]

TEM surveying results of Ag–Ni samples synthesized from glycol solutions at 90 °C using both (a) microwave *E*-field and (b) *H*-field irradiation is shown in Fig. 6. These images indicate that the suspension resulting from *H*-field irradiation contained mono-disperse nanoparticles having a size distribution of 4.4 ± 2.1 nm. By contrast, particles synthesized by *E*-field irradiation had a wider distribution of the particle size than the *H*-field irradiated sample even though the measured bulk temperature was the same in both experimental runs.

The chemical composition of the synthesized nanoparticles was determined employing TEM-EDS measurements. The images are given as Fig. 7 for the Ag–Al (a-(i), (ii) and (iii)), the Pd–Ag (b-(i), (ii) and (iii)), and the Ag–Ni (c-(i), (ii) and (iii)) system. Firstly, the bright field image of TEM (a-(i)) and the EDS results (a-(ii) and a-(iii)) for the Ag–Al system revealed that only pure Ag particles were formed during the microwave assisted polyol process employed here. The element Al was not incorporated into the particles and is only dispersed on the grid used as sample holder during these measurements.

On the other hand, the TEM-EDS results presented in Fig. 7(b) and (c) show that Ag as well as Pd and Ni are uniformly distributed on the surface of the nanoparticles, thus, clearly evincing the formation of bimetallic Pd–Ag and Ag–Ni nanoparticles by the microwave irradiation of ethylene glycol solutions of $[Ag(NH_3)_2]^+/Pd(NO_3)_2$ and $[Ag(NH_3)_2]^+/Ni(NO_3)_2$, respectively. No significant differences of the composition of the respective alloys formed by irradiation in the microwave *E*-field and *H*-field are observed.

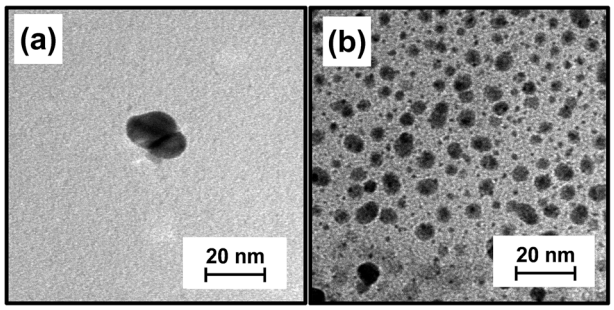

Fig. 6 TEM images of Ag–Ni nanoparticles synthesized at 90 °C under microwave (a) *E*-field and (b) *H*-field condition.

The reduction of ions of noble metals such as Ag and Pd dissolved in a solution of ethylene glycol and a capping agent such as PVP is known to proceed slowly at ambient temperature. To achieve almost complete conversion a reaction time of several days is required as was reported for the polyol syntheses of silver and palladium nanoparticles.[38]

For synthetic purposes the reduction of Ag^+ in the presence of ethylene glycol, PVP, and dissolved molecular oxygen requires temperatures exceeding 120 °C.[39] The formation of Ag nanoparticles by polyol syntheses in the presence of ethylene glycol is said to be initiated by the thermal oxidation of the diol at temperatures >120 °C yielding glycolaldehyde as the primary reducing agent of Ag^+. The Ag nanoparticles formed are catalyzing the oxidation of ethylene glycol to glycolaldehyde, thus accelerating the formation rate of the nanoparticles.[40] Consequently, Ag nanoparticles are formed in a polyol process at temperatures significantly lower than 120 °C only in the presence of seed particles.[41] The formation of Pd nanoparticles by polyol syntheses is known to occur at lower temperatures than the syntheses of Ag nanoparticles.[38,42–44] It has been reported that metallic palladium is formed in a slow process at room temperature upon dissolution of Pd nitrate in ethylene glycol indicating that free Pd(II) ions are instantaneously reduced by this solvent to the elemental metal.[35] On the other hand, it is known as well that the synthesis of Ni nanoparticles by reduction of Ni^{2+} in the presence of a glycol as the reducing agent requires higher temperatures than the reduction of Ag^+. Usually the reactions are performed at temperatures of 190 °C or higher, and Pt or other noble metal salts are added to form seeds for the Ni nanoparticles formation.[15,45–47] The presence of hydroxide anions in the polyol solution is known to accelerate the formation of Ag, Pd, and Ni nanoparticles at ambient as well as at elevated temperatures.[48,49] As well, the presence of NH_3 is known to affect the formation kinetics of metal nanoparticles. It was shown that when $Pd(NH_3)_4(NO_3)_2$ is used as the precursor to synthesize palladium metal, its dissolution in ethylene glycol was not followed by the reduction of Pd(II) species at ambient temperature. Heating the palladium solution up to 100 °C resulted in the formation of colloidal palladium. It was assumed that complexation of Pd(II) by ammonia stabilizes the metal species against reduction by ethylene glycol at ambient temperature. At higher temperature the formation of palladium metal may be induced by the thermal decomposition of the palladium–ammine complex followed by subsequent reduction of the free palladium by ethylene glycol.[38] Here, the ethylene glycol solution contained an excess of ammonia (Mar ratio $Ag(NH_3)_2^+ : M^{n+} : NH_3 = 1.0 : 0.72 : 15$) and of hydroxide anions. It can be assumed that under these conditions a mixture of free metal ions in equilibria with complexes of NH_3 and polyol[50,51] are initially present in the solution. Complexation of the metal ions by PVP need not be considered.[52]

The color of a sole $Ag(NH_3)_2^+$ solution in an ethylene glycol/PVP mixture changed only after 72 hours of storage at ambient temperature (Fig. 8(a)) indicating a slow formation of Ag nanoparticles. The absorption spectra of microwave irradiated $Ag(NH_3)_2^+$ solutions in ethylene glycol recorded directly after reaching the indicated temperature as shown in Fig. 8(b). It

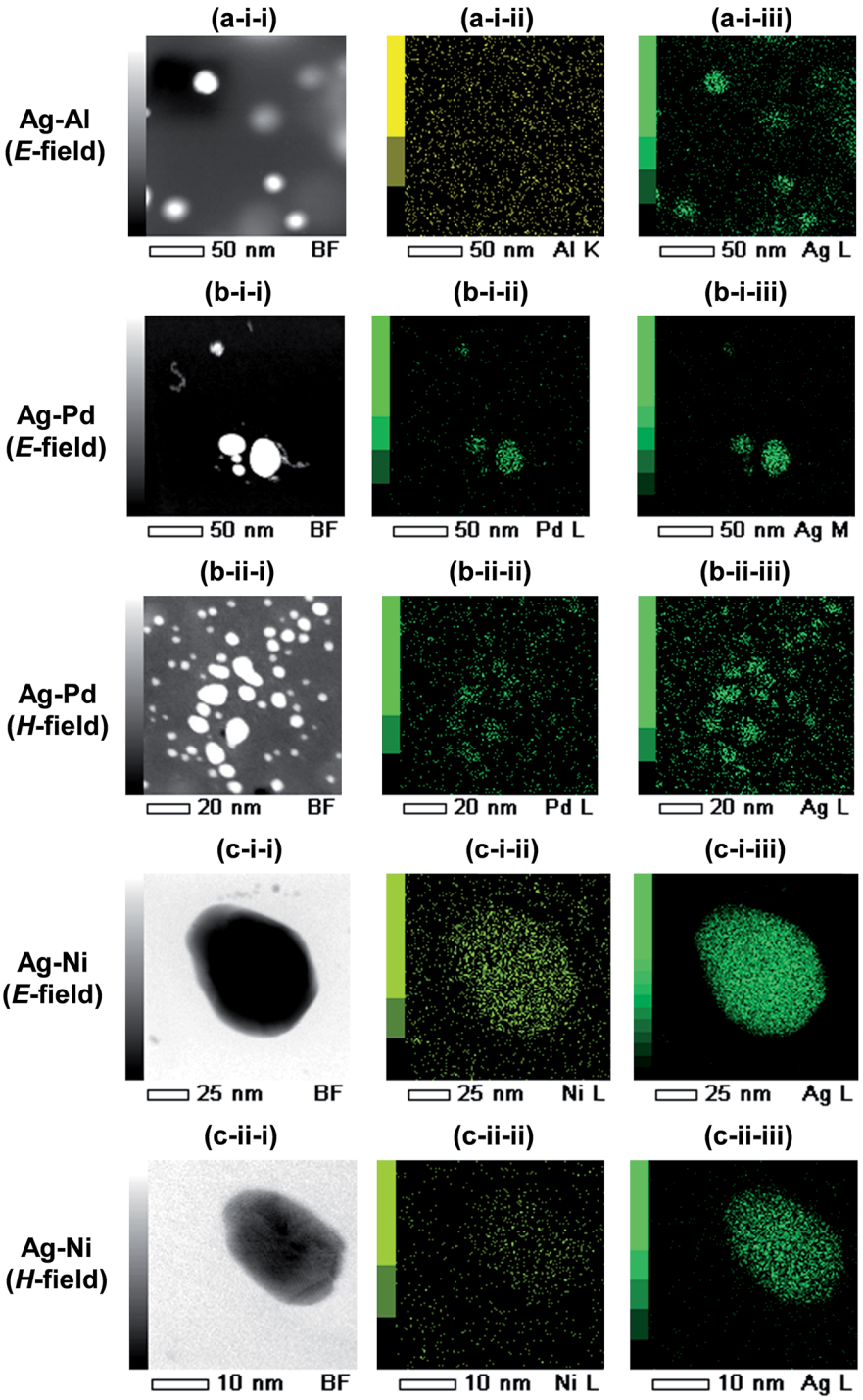

Fig. 7 TEM-EDS map images of nanoparticles containing Ag and other metals prepared at (a) 130 °C and (b, c) 80 °C.

becomes obvious that at temperatures exceeding 100 °C the reduction of $Ag(NH_3)_2^+$ becomes a rapid process resulting in the formation of Ag nanoparticles. Microwave irradiation results in energy absorption in the bulk of the reacting solution resulting in the formation of small metal clusters known to autocatalyse the reduction process.[37] The results obtained in the experimental runs performed at ambient temperature (Fig. 8(a)) suggest that the formation of silver clusters is slowly initiated at low temperatures. Higher temperatures are accelerating this particle formation process resulting in shorter time intervals until the observable appearance of the plasmon resonance. As shown here, the formation of pure Ag nanoparticles succeeds under microwave irradiation at temperatures >100 °C with reaction rates reasonable for synthetic purposes (Fig. 4(a) and 8(b)).

At ambient temperature we assume the very slow reduction of (complexed) Ag^+ forming a silver atom (eqn (3) with $n = 1$)

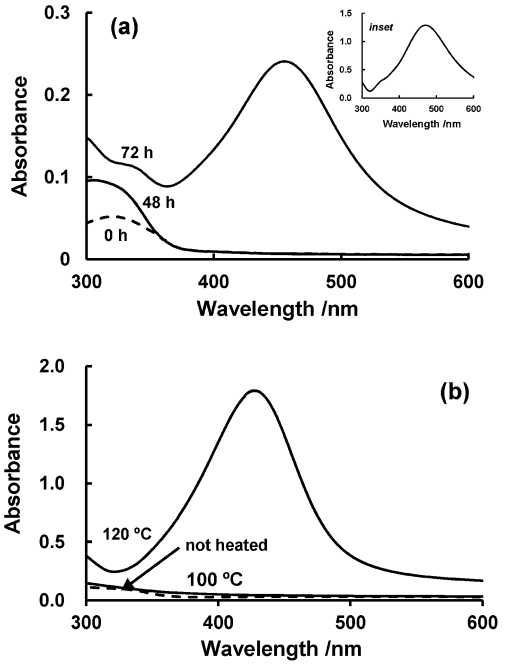

Fig. 8 UV-vis spectra of solutions of $Ag(NH_3)_2^+$ in ethylene glycol containing dissolved molecular oxygen during (a) storage at ambient temperature, and (b) heating from ambient temperature to 100 and 120 °C by microwave irradiation. The inset in (a) shows the spectrum after storage for 72 hour in an O_2-free solution (Ar atmosphere).

followed by the adsorption of an additional Ag ion (eqn (4) with $n = 1$) and its subsequent reduction yielding Ag_2 (eqn (5) with $n = 1$).[53] In subsequent reaction steps Ag^+ is adsorbed at the surface of the silver clusters and reduced by electron transfer from an oxidizable organic species present in the reacting mixture (eqn (4) and (5) with $n \geq 2$) resulting in the formation of Ag nanoparticles after prolonged reaction time at ambient temperature.

$$Ag_n^+ + e^- \rightarrow Ag_n \quad (3)$$

$$Ag_n + Ag^+ \rightarrow Ag_{n+1}^+ \quad (4)$$

$$Ag_{n+1}^+ + e^- \rightarrow Ag_{n+1} \quad (5)$$

The probability of the direct reduction of $Ag(NH_3)_2^+$ seems to be low due to thermodynamic reasons (reduction potential). As shown in Fig. 4(a) and (b) the increase of the Ag content at constant ammonia concentration in the polyol solution facilitates the formation of nanoparticles at significantly lower temperature (105 °C *vs.* 120 °C for the $[Ag(NH_3)_2]^+$-containing solution). It is likely that more uncomplexed Ag ions are available for the reduction reaction thus allowing the formation of particles at a significantly lower temperature.

The increase of the temperature is obviously resulting in an increase of the formation rate of the Ag nanoparticles. However, the question which reaction step is accelerated cannot be answered on the basis of the experimental results presented here. These experimental results, however, allow the conclusion that small Ag clusters are formed even at temperatures well below 120 °C, and that the formation of glycolaldehyde (known to by thermal oxidation of the diol at temperatures >120 °C)[37] is not a prerequisite to initiate the reduction process of Ag^+.

As has been mentioned above, the reduction of Pd^{2+} in a polyol process occurs at lower temperatures than the reduction of Ag^+. Since no electron transfer occurs between Pd^+ and Ag^+ (ref. 54) it is, therefore, assumed that the formation of the Pd–Ag bimetallic particles is initiated by the reductive formation of Pd seed particles (eqn (6)–(9)). The formation of Pd seeds induces the growth of alloy particles (eqn (10) and (11)).

$$Pd^{2+} + e^- \rightarrow Pd^+ \quad (6)$$

$$2Pd^+ \rightarrow Pd^0 + Pd^{2+} \quad (7)$$

$$Pd^0 + Pd^+ \rightarrow Pd_2^+ \quad (8)$$

$$Pd_2^+ + e^- \rightarrow Pd_2 \quad (9)$$

$$Pd^0 + Ag^+ \rightarrow PdAg^+ \quad (10)$$

$$PdAg^+ + e^- \rightarrow PdAg \quad (11)$$

Under the experimental conditions employed in this work, the formation of Ag–Ni nanoparticles was observed to occur at a temperature of 80 °C (*cf.* Fig. 5(a)). Irradiation of Ni^{2+}/NH_3 in a mixture of ethylene glycol and PVP in the microwave *E*-field resulted in temperatures >120 °C but no nanoparticles were formed (data not shown). Therefore, it can be assumed that small Ag clusters (Ag_{n+1}) are formed in initial reaction steps (eqn (3)–(5)) at bulk temperatures ≤80 °C catalyzing the reduction of adsorbed Ni^{2+} or Ni^+ (eqn (12) and (13)).

$$Ag_{n+1} + Ni^{m+} \rightarrow Ag_{n+1}Ni^{m+} \quad (12)$$

$$Ag_{n+1}Ni^{m+} + me^- \rightarrow Ag_{n+1}Ni \quad (13)$$

Competition between Ni^{2+} (or Ni^+) and Ag^+ for electrons in later reaction steps after depletion of Ag^+ in the solution results in Ag–Ni alloy formation by statistical reasons.

The reaction of Ni species according to

$$Ni^{2+} + e^- \rightarrow Ni^+ \quad (14)$$

$$2Ni^+ \rightarrow Ni^{2+} + Ni^0 \quad (15)$$

$$Ni^+ + Ag^+ \rightarrow Ni^{2+} + Ag^0 \quad (16)$$

in an early stage of the reaction sequence can be excluded since Ni^+ neither disproportionates nor reacts with Ag^+.[55,56] In comparison with the $[Ag(NH_3)_2]^+/Ag^+$ mixture the reaction temperature necessary for rapid nanoparticle formation from $[Ag(NH_3)_2]^+/Ni^{2+}$ solutions is lower. Following the argument given above it is assumed that the Ni^{2+} is reacting with NH_3 yielding $[Ni(NH_3)_6]^{2+}$ and thus increasing the concentration of uncomplexed Ag ions. A significant amount of these ions are then available for the reduction reaction already at the low temperature of 80 °C.

In the above discussion the experimental results are explained with pure physical (heating rate, temperature) and chemical phenomena (temperature-dependent complex stability and reduction potential). However, these models do not explain the observed difference in the particle size distribution of the Ag–Ni particles synthesized in the microwave *E*- and *H*-field (*cf.* Fig. 6). Ni^{2+} ions are known to be paramagnetic and Ag–Ni alloys exhibit weak paramagnetic to ferromagnetic behavior depending on its composition.[57] Therefore, a strong interaction between the magnetic field and Ni^{2+} resulting in rapid nucleation is assumed. The resulting AgNi nanoparticles may cause local overheating of the reaction mixture due to a strong interaction between the particles and the *H*-field. This effect is less pronounced in the case of Pd particles which are also known to interact with the *H*-field since the large magnetic susceptibility of Pd is decreasing during alloy formation with increasing Ag content.[58,59] Therefore, the formation of small AgNi nanoparticles in the microwave *H*-field is possibly the result of a specific microwave effects.

Conclusions

The synthesis of mono-disperse (alloy) nanoparticles has been performed using a wet process of glycol solutions containing $[Ag(NH_3)_2]^+$ and a second metal cation M^{n+} (M = Ag, Na, Al, Ni or Pd) under microwave irradiation in a predominately electric or a predominately magnetic field. The formation of pure Ag nanoparticles with a reaction rate suitable for synthetic purposes required a temperature higher 100 °C while Ag–Ni and Pd–Ag alloys were formed at a significantly lower temperature of only 80 °C. Under the experimental conditions used here, temperatures exceeding 85 °C were accessible under microwave *E*-field irradiation, *i.e.*, Ag nanoparticles were only formed in the microwave *E*-field while Ag–Ni and Pd–Ag nanoparticles were formed in the *E*-field as well as in the *H*-field. Differences in the rate of product formation solely resulted from differences in the chemical reactivity of the involved metal cations and the temperature of the reacting solution. No specific effects of the microwave *E*-field and *H*-field on the rate of product formation have been observed. The synthesis of Ag–Ni alloy particles in the *E*-field and the *H*-field resulted in products with different particle size, thus possibly indicating specific field effects.

Acknowledgements

S.H. is grateful to the Japan Society for the Promotion of Science for financial support (JSPS; Grant-in-aid for Scientific Research no. C-25420820). S.T. is grateful to the Sasakawa for financial support. A grant from the Sophia University-wide Collaborative Research Fund to S.H. is also appreciated. R.D. thanks the Gottfried Wilhelm Leibniz University Hannover, Germany, and Prof. Dr D. Bahnemann for granting him a leave of absence.

Notes and references

1 R. J. Giguere, T. L. Bray, S. M. Duncan and G. Majetich, *Tetrahedron Lett.*, 1986, **27**, 4945–4948.
2 R. Gedye, F. Smith, K. Westaway, H. Ali, L. Baldisera, L. Laberge and J. Rousell, *Tetrahedron Lett.*, 1986, **27**, 279–282.
3 P. Lidström, J. Tierney, B. Wathey and J. Westman, *Tetrahedron*, 2001, **57**, 9225–9283.
4 A. de la Hoz and A. Loupy, *Microwaves in organic synthesis*, Wiley-VCH-Verl, Weinheim, 3rd edn, 2012.
5 *Microwaves in Nanoparticle Synthesis. Fundamentals and Applications*, ed. S. Horikoshi and N. Serpone, Wiley-VCH, Weinheim, 1st edn, 2013.
6 F.-K. Liu, C.-J. Ker, Y.-C. Chang, F.-H. Ko, T.-C. Chu and B.-T. Dai, *Jpn. J. Appl. Phys.*, 2003, **42**, 4152–4158.
7 M. Tsuji, M. Hashimoto, Y. Nishizawa and T. Tsuji, *Mater. Lett.*, 2004, **58**, 2326–2330.
8 S. Kundu, L. Peng and H. Liang, *Inorg. Chem.*, 2008, **47**, 6344–6352.
9 S. Horikoshi, H. Abe, T. Sumi, K. Torigoe, H. Sakai, N. Serpone and M. Abe, *Nanoscale*, 2011, **3**, 1697–1702.
10 S. Komarneni, D. Li, B. Newalkar, H. Katsuki and A. S. Bhalla, *Langmuir*, 2002, **18**, 5959–5962.
11 S. Komarneni, H. Katsuki, D. Li and A. S. Bhalla, *J. Phys.: Condens. Matter*, 2004, **16**, S1305.
12 F.-K. Liu, P.-W. Huang, T.-C. Chu and F.-H. Ko, *Mater. Lett.*, 2005, **59**, 940–944.
13 S. Horikoshi, H. Abe, K. Torigoe, M. Abe and N. Serpone, *Nanoscale*, 2010, **2**, 1441–1447.
14 M. Tsuji, M. Hashimoto and T. Tsuji, *Chem. Lett.*, 2002, 1232–1233.
15 D. Li and S. Komarneni, *J. Am. Ceram. Soc.*, 2006, **89**, 1510–1517.
16 W. Xu, K. Y. Liew, H. Liu, T. Huang, C. Sun and Y. Zhao, *Mater. Lett.*, 2008, **62**, 2571–2573.
17 I. Bilecka, L. Luo, I. Djerdj, M. D. Rossell, M. Jagodič, Z. Jagličić, Y. Masubuchi, S. Kikkawa and M. Niederberger, *J. Phys. Chem. C*, 2011, **115**, 1484–1495.
18 I. Belecka, A. Hintennach, I. Djerdj, P. Nocak and M. Niederberger, *J. Mater. Chem.*, 2009, **19**, 5125–5128.
19 I. Belecka, I. Djerdj and M. Niederberger, *Chem. Commun.*, 2008, **7**, 886–888.
20 M. Tsuji, M. Hashimoto, Y. Nishizawa, M. Kubokawa and T. Tsuji, *Chem.–Eur. J.*, 2005, **11**, 440–452.
21 M. Tsuji, S. Hikino, M. Matsunaga, Y. Sano, T. Hashizume and H. Kawazumi, *Mater. Lett.*, 2010, **64**, 1793–1797.
22 M. Tsuji, S. Hikino, R. Tanabe, M. Matsunaga and Y. Sano, *CrystEngComm*, 2010, **12**, 3900.
23 Z. Chen, D. Mochizuki and Y. Wada, in [5], pp. 145–183.
24 S. Horikoshi, T. Sumi and N. Serpone, *J Microwave Power Electromagnetic Energy*, 2012, **46**, 215–228.
25 N. J. Cronin, *Microwave and optical waveguides*, Institute of Physics Publ., Bristol, 1995.
26 S. Horikoshi, A. Matsubara, S. Takayama, M. Sato, F. Sakai, M. Kajitani, M. Abe and N. Serpone, *Appl. Catal., B*, 2009, **91**, 362–367.
27 D. M. Pozar, *Microwave engineering*, Wiley, Hoboken, NJ, 3rd edn, 2004.
28 S. Horikoshi and N. Serpone, *J. Photochem. Photobiol., C*, 2009, **10**, 96–110.

29 H. Xu and M. Käll, *Sens. Actuators, B*, 2002, **87**, 244–249.
30 H. Xu and M. Käll, *Phys. Rev. Lett.*, 2002, **89**, 246802.
31 T. Tsuji, D.-H. Thang, Y. Okazaki, M. Nakanishi, Y. Tsuboi and M. Tsuji, *Appl. Surf. Sci.*, 2008, **254**, 5224–5230.
32 C. M. Cobley, S. E. Skrabalak, D. J. Campbell and Y. Xia, *Plasmonics*, 2009, **4**, 171–179.
33 K. Nouneh, M. Oyama, R. Diaz, M. Abd-Lefdil, I. V. Kityk and M. Bousmina, *J. Alloys Compd.*, 2011, **509**, 5882–5886.
34 Z. Zhang, T. M. Nenoff, K. Leung, S. R. Ferreira, J. Y. Huang, D. T. Berry, P. P. Provencio and R. Stumpf, *J. Phys. Chem. C*, 2010, **114**, 14309–14318.
35 A. Henglein, *Chem. Mater.*, 1998, **10**, 444–450.
36 K. Patel, S. Kapoor, D. P. Dave and T. Mukherjee, *J. Chem. Sci.*, 2005, **117**, 311–316.
37 W. Wang and G. Cao, *J. Nanopart. Res.*, 2007, **9**, 1153–1161.
38 F. Bonet, V. Delmas, S. Grugeon, R. Herrera Urbina, P.-Y. Silvert and K. Tekaia-Elhsissen, *Nanostruct. Mater.*, 1999, **11**, 1277–1284.
39 B. Wiley, Y. Sun and Y. Xia, *Acc. Chem. Res.*, 2007, **40**, 1067–1076.
40 S. E. Skrabalak, B. J. Wiley, M. Kim, E. V. Formo and Y. Xia, *Nano Lett.*, 2008, **8**, 2077–2081.
41 Y. Sun, B. Mayers, T. Herricks and Y. Xia, *Nano Lett.*, 2003, **3**, 955–960.
42 F. Chen, Z. Zhong, X.-J. Xu and J. Luo, *J. Mater. Sci.*, 2005, **40**, 1517–1519.
43 Y. Xiong, H. Cai, B. J. Wiley, J. Wang, M. J. Kim and Y. Xia, *J. Am. Chem. Soc.*, 2007, **129**, 3665–3675.
44 S. E. Skrabalak, J. Chen, Y. Sun, X. Lu, L. Au, C. M. Cobley and Y. Xia, *Acc. Chem. Res.*, 2008, **41**, 1587–1595.
45 U. N. Tripathi, A. Soni, V. Ganesan and G. S. Okram, in *Solid State Physics: Proc. 56th DAE Solid State Physics Symposium 2011, AIP*, 2012, pp. 437–438.
46 K. J. Carroll, J. U. Reveles, M. D. Shultz, S. N. Khanna and E. E. Carpenter, *J. Phys. Chem. C*, 2011, **115**, 2656–2664.
47 M. Blosi, S. Albonetti, A. L. Costa, N. Sangiorgi and A. Sanson, *Chem. Eng. J.*, 2013, **215–216**, 616–625.
48 Z. Y. Huang, G. Mills and B. Hajek, *J. Phys. Chem.*, 1993, **97**, 11542–11550.
49 T. Hinotsu, B. Jeyadevan, C. N. Chinnasamy, K. Shinoda and K. Tohji, *J. Appl. Phys.*, 2004, **95**, 7477–7479.
50 S. Nam, D. V. Parikh, B. D. Condon, Q. Zhao and M. Yoshioka-Tarver, *J. Nanopart. Res*, 2011, **13**, 3755–3764.
51 C. Luo, Y. Zhang, X. Zeng, Y. Zeng and Y. Wang, *J. Colloid Interface Sci.*, 2005, **288**, 444–448.
52 M. Liu, X. Yan, H. Liu and W. Yu, *React. Funct. Polym.*, 2000, **44**, 55–64.
53 A. Henglein, *Ber. Bunsenges. Phys. Chem.*, 1977, **81**, 556–561.
54 H. Remita, M. Tréguer, J. Amblard, J. Belloni and J. Khatouri, *Z. Phys. D: At., Mol. Clusters*, 1997, **40**, 127–130.
55 M. Kelm, J. Lilie, A. Henglein and E. Janata, *J. Phys. Chem.*, 1974, **78**, 882–887.
56 B. G. Ershov, E. Janata and A. Henglein, *J. Phys. Chem.*, 1994, **98**, 7619–7623.
57 K. Santhi, E. Thirumal, S. N. Karthick, H.-J. Kim, M. Nidhin, V. Narayanan and A. Stephen, *J. Nanopart. Res.*, 2012, DOI: 10.1007/s11051-012-0868-7.
58 F. E. Hoare, J. C. Matthews and J. C. Walling, *Proc. R. Soc. London, Ser. A*, 1953, **216**, 502–515.
59 W. Sänger and J. Voitländer, *Z. Phys. B: Condens. Matter*, 1981, **44**, 283–291.